Journal Pre-proof

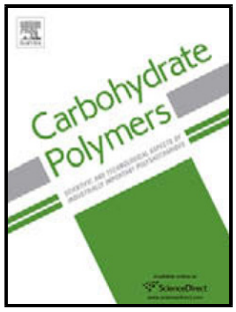

Colloidal features of softwood galactoglucomannans-rich extract

Mamata Bhattarai (Conceptualization) (Methodology) (Investigation) (Formal analysis) (Visualization)<ce:contributor-role>Writing-original draft), Irina Sulaeva (Methodology) (Formal analysis) (Validation)<ce:contributor-role>Writing-Review and Editing), Leena Pitkänen (Conceptualization) (Formal analysis) (Validation)<ce:contributor-role>Writing-Review and Editing), Inkeri Kontro (Investigation) (Formal analysis)<ce:contributor-role>Writing-Review and Editing), Maija Tenkanen (Conceptualization) (Methodology)<ce:contributor-role>Writing-Review and Editing), Antje Potthast (Methodology) (Supervision)<ce:contributor-role>Writing-Review and Editing), Kirsi S. Mikkonen (Conceptualization) (Supervision)<ce:contributor-role>Writing-Review and Editing)

PII:	S0144-8617(20)30542-7
DOI:	https://doi.org/10.1016/j.carbpol.2020.116368
Reference:	CARP 116368
To appear in:	*Carbohydrate Polymers*
Received Date:	29 January 2020
Revised Date:	17 April 2020
Accepted Date:	23 April 2020

Please cite this article as: Bhattarai M, Sulaeva I, Pitkänen L, Kontro I, Tenkanen M, Potthast A, Mikkonen KS, Colloidal features of softwood galactoglucomannans-rich extract, *Carbohydrate Polymers* (2020), doi: https://doi.org/10.1016/j.carbpol.2020.116368

Colloidal features of softwood galactoglucomannans-rich extract

Mamata Bhattarai[1], Irina Sulaeva[2], Leena Pitkänen[1+], Inkeri Kontro[3], Maija Tenkanen[1], Antje Potthast[2], Kirsi S.Mikkonen[1,4]*

[1] Department of Food and Nutrition, University of Helsinki, Finland

[2] Department of Chemistry, University of Natural Resources and Life Sciences, Austria

[3] Department of Physics, University of Helsinki, Finland

[4] Helsinki Institute of Sustainability Science, University of Helsinki, Finland

[+] Present address: Department of Bioproducts and Biosystems, Aalto University, Finland

Graphical abstract

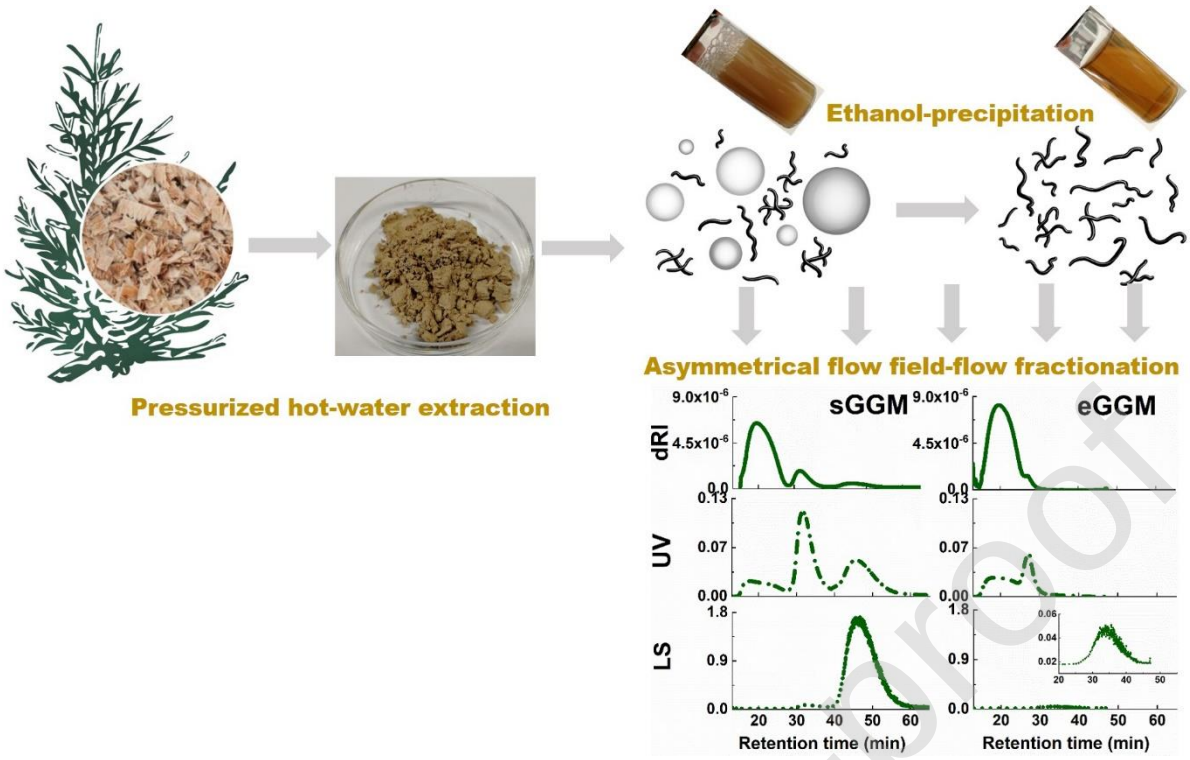

Research highlights

- Macromolecular analysis of spruce galactoglucomannans (GGM)-rich extract was performed.
- AF4 parameters for efficient fractionation of crude polysaccharide extract were studied.
- GGM extracts were found be a colloidal mixture of polysaccharides and particles/aggregates.
- Presence of colloidal particles depended on purity of GGM extract.

ABSTRACT

Development of a sustainable bioeconomy requires valorization of renewable resources, such as wood hemicelluloses. The intra- and inter-molecular associations of hemicelluloses within themselves or with other wood components can result in complex macromolecular features. These features exhibit functionality as hydrocolloids, however macromolecular characterization of these heterogeneous materials are challenging using conventional techniques such as size-exclusion chromatography. We studied galactoglucomannans (GGM) -rich softwood extracts at two grades of purity—as crude extract and after ethanol-precipitation. Asymmetrical flow field-flow fractionation (AF4) was optimized and utilized to fractionate size classes in GGM extracts, and subsequent characterization was performed with light scattering and microscopy techniques. Both GGM extracts contained polysaccharides of around 10,000 g/mol molar mass, and colloidal assemblies and/or particles in sub-micron size range. The optimized AF4 method facilitates the characterization of complex biomass-derived carbohydrates without pre-fractionation, and provides valuable understanding of their unique macromolecular features for their future application in food, pharmaceuticals, and cosmetics.

KEYWORDS: asymmetrical flow field-flow fractionation, wood hemicelluloses, galactoglucomannans, particles, aggregates

1. Introduction

Polysaccharides from plants (such as starch from grains), animals (such as chitin from shellfish), and microbes (such as xanthan gum from *Xanthomonas campestris*) are industrially important carbohydrate polymers. They are commonly isolated and converted for use as emulsifiers, texture enhancers, film forming agents, and delivery vehicles in the areas of food, cosmetics, pharmaceuticals, and coatings, and in other technical applications (Dickinson, 2017).

The transition from an oil-based economy to a bioeconomy increases demand of renewable and technologically superior polysaccharides for use in functional materials (Employment, 2017). Significant value lies in the valorization of hemicelluloses from lignocellulosic biomass. The predominant hemicelluloses in common softwood species, Norway spruce (*Picea abies*) are galactoglucomannans (GGM). GGM are composed of backbones with partially acetylated β(1→4)-linked Man*p* and Glc*p* units, substituted by α (1→6)-linked Gal*p* (Sjöström, 1993). GGM were first recovered in both laboratory and semi-pilot scale studies from the process water of thermo-mechanical pulping (TMP) processes (Willför, Rehn, Sundberg, Sundberg, & Holmbom, 2003; Xu,

Willfor, Sundberg, Pettersson, & Holmbom, 2007). They can also be extracted from wood chips or saw dust prior to pulping using pressurized hot water extraction (Kilpeläinen et al., 2014; Schoultz, 2015), microwave heat (Söderqvist Lindblad, Ranucci, & Albertsson, 2001), steam explosion (Chadni, Grimi, Bals, Ziegler-Devin, & Brosse, 2019; Jedvert, Saltberg, Lindström, & Theliander, 2012), and high voltage electrical discharge (Chadni, Grimi, Ziegler-Devin, Brosse, & Bals, 2019). In the past decade, GGM research has shifted from characterizing their role in pulping and paper making to the development of high-value added materials for techno-functional applications. They have been studied as film-forming agents (Lindblad, Dahlman, Sjöberg, & Albertsson, 2009; Mikkonen, Heikkilä, Willför, & Tenkanen, 2012), hydrogels (Al-Rudainy, Galbe, Arcos Hernandez, Jannasch, & Wallberg, 2019; Söderqvist Lindblad et al., 2001), aerogels (Alakalhunmaa et al., 2016) and recently as very promising hydrocolloid with multifunctional emulsification and stabilization abilities for food and alkyd paint emulsions (Bhattarai et al., 2019; Lehtonen et al., 2018; Lehtonen et al., 2016; Mikkonen et al., 2019; Mikkonen, Merger, et al., 2016; Mikkonen, Xu, Berton-Carabin, & Schroën, 2016; Valoppi et al., 2019).

Hemicelluloses are present in the secondary cell walls of wood, embedded together with cellulose and lignin. Thus, lignin-derived compounds are commonly co-extracted with hemicelluloses. In a previous study, lignin residues were responsible for the formation of wood xylan aggregates (Westbye, Köhnke, Glasser, & Gatenholm, 2007). In Pressurized hot water extracted GGM (PHWE GGM) co-eluted lignin were assumed to form GGM-lignin particles (Valoppi et al., 2019). In PHWE GGM, formation of GGM aggregates was also hypothesized to be induced by lignin residues (Bhattarai et al., 2020). In dispersed systems, these colloidal features may induce Pickering-type stabilization (Bhattarai et al., 2019; Mikkonen, Merger, et al., 2016; Valoppi et al., 2019) analogous to stabilization mechanism by starch granules, chitin, and cellulose nanocrystals (Dickinson, 2017). In polysaccharides, colloidal features in the form of macromolecular or supramolecular aggregates

and particles are a result of partial solubility or insolubility, which is a complex thermodynamic balance between the inherent properties of polysaccharide and medium (Guo, Hu, Wang, & Ai, 2017). Even minor amounts of co-components, like protein or phenolic compounds, can greatly affect the solubility of polysaccharide extracts (Ebringerová, Hromádková, & Heinze, 2005). This consequently affects their techno-functional properties, e.g., emulsifying, stabilizing, and film-forming capacity (Harding, 2005), augmenting the importance of their characterization.

To apply complex lignocellulose extracts in materials, their macromolecular and colloidal properties, such as molar mass and conformation in aqueous state must be known; however, their characterization is very challenging due to limitations in existing techniques. The overall solubility of hemicellulose-rich extracts can be altered by the presence of bound or free form lignin. Lignin forms colloidal particles due to poor solubility in aqueous solvents. Characterization of these colloidal features adds to the existing challenges in polysaccharide characterization, which include molar mass dispersity and high branching degree (Zielke, Fuentes, Piculell, & Nilsson, 2018). Conventionally employed size-exclusion chromatography (SEC) requires mandatory sample pre-filtration, resulting in loss of high molar-mass colloidal fraction. Even after sample filtration, there is a risk of colloidal structures block the costly SEC columns (Podzimek, 2011; Zielke et al., 2018). With SEC, there is also a high possibility of structure deformation due to shear degradation (Podzimek, 2011). Asymmetrical flow field-flow fractionation technique (AF4) largely overcomes these problems. In AF4, the absence of a stationary phase allows for the injection of non-filtered samples without the risk of channel blockage. This result in a comprehensive analysis of samples with broad distributions such as crude polysaccharide extracts, without the discrimination of the large molar mass fractions and aggregates. AF4 is highly suited for understanding the complex macromolecular features of polysaccharides when coupled to detectors, such as multi-angle light scattering (MALS), dynamic light scattering,

and refractive index (RI) (Pitkänen, Tenkanen, & Tuomainen, 2011; Runyon, Ulmius, & Nilsson, 2014; Zielke et al., 2018).

We hypothesize that GGM-rich extracts in aqueous solution contain a mixture of individual polysaccharide molecules with an average molar mass around 10,000 g/mol as reported by previous studies (Bhattarai et al., 2019; Mikkonen, Merger, et al., 2016; Valoppi et al., 2019) and entities of higher structural order, e.g., aggregates and/or particles. Consequently, size dispersity due to differences in conformation is hypothesized. In our previous studies, we have estimated the particle size of GGM extracts using offline dynamic light scattering method (Bhattarai et al., 2020; Valoppi et al., 2019). However, this method has poor separation resolution and does not distinguish conformational features. The aim of the present work was to address two challenges of current biorefineries. First, to facilitate the characterization of crude polysaccharide extracts using AF4, and second, to provide comprehensive details of the macromolecular features of GGM extracts and thus facilitate their application as novel biomass-based materials. We aimed to optimize the method and fractionate multiple size classes present in PHWE GGM extracts using AF4 and characterize their molar mass and conformational properties using a combination of techniques: MALS, small-angle X-ray scattering (SAXS) and cryo-transmission electron microscopy (Cryo-TEM). To our understanding, this is the first study that has characterized crude GGM extract using AF4.

2. Materials and methods

2.1 Sample preparation

GGM were extracted from spruce sawdust using the PHWE process in a pilot-scale flow-through extraction system (Kilpeläinen et al., 2014). Briefly, the spruce sawdust was extracted at 170 °C for 70 min at a flow rate of 20 mL/min using tap water. The crude extract was either spray-dried to obtain sGGM or ethanol precipitation was performed as described in our previous study (Bhattarai et al., 2019) to obtain eGGM. Spray drying was performed using a Buchi Mini Spray Dryer B-290 (Buchi,

Switzerland) at an inlet temperature of 170 °C and an outlet temperature of 65 °C with dry air at a flow rate of 667 l/h. The sGGM and eGGM were obtained in powder form and stored at RT protected from light.

Both GGM extracts had heterogeneous monosaccharide composition: 55–60% mannose, 14–15% glucose, 10–14% xylose, 7–10% galactose, around 3% galacturonic acid, 2.5–3.5% methyl-glucuronic acid, and less than 1% arabinose and rhamnose (Bhattarai et al., 2019; Mikkonen et al., 2019; Valoppi et al., 2019). All percentages were based on dry GGM extract. sGGM and eGGM had about 73 wt% (Valoppi et al., 2019) and 86 wt% (Bhattarai et al., 2019) total carbohydrate content, respectively, which was calculated by summing up the monosaccharides and correcting for the condensation reaction with correction factors 0.88, 0.9 and 0.91 for pentoses, hexoses and uronic acids, respectively. The monosaccharide analysis was performed by acid methanolysis followed by gas chromatography (Sundberg, Sundberg, Lillandt, & Holmhom, 1996). The phenolic content of sGGM was 40–50 (Mikkonen et al., 2019; Valoppi et al., 2019) and that of eGGM was 16 (Valoppi et al., 2019) Gallic acid equivalent/g of dry GGM. The amount of extractives in sGGM and eGGM were 5.1 and 0.4 mg/g, respectively (Mikkonen et al., 2019). A detailed chemical characterization of the phenolic compounds and extractives has been performed in our recent study (Mikkonen et al., 2019).

Aqueous solutions of GGM extracts were prepared at concentrations of 5 and 10 mg/mL in 25 mM sodium citrate buffer at pH 4.5 by dissolving overnight with mild shaking. Sodium azide was added at 250 ppm to prevent microbial spoilage.

Reagents used were citric acid monohydrate, sodium hydroxide, and sodium azide, all from Merck (Darmstadt, Germany). Deionized water or HPLC-grade water from Merck (Darmstadt, Germany) was used for sample preparation. HPLC-grade water was used to prepare AF4 eluent.

2.2 Instrumental setup for AF4

The AF4 setup used the Dionex DG-1210 online degasser, an Agilent Technologies 1260 Infinity Pump, an Agilent Technologies G1367C autosampler, and an Eclipse AF4 separation system (Wyatt Technologies, Santa Barbara, USA). Separation of GGM occurred in a 275 mm long separation channel with a 350 μm or 490 μm spacer. The separation system was coupled sequentially to a UV detector (Azura UVD 2.1S, KNAUER GmbH, Germany) set at 280 nm; a Wyatt DAWN HELEOS II MALS detector equipped with a 658 nm laser and band-pass filters installed on each second of 18 detectors; and a Wyatt TReX refractive index (dRI) detector. Band-pass filters are necessary when fluorescence-emitting compounds are present in the sample, such as lignin or lignin-derived phenolic residues in our case. All detectors were set at 25 °C, whereas the separation channel was at RT (22–23 ºC). The MALS data was evaluated by Astra 6.1 (Wyatt Technology). The obtained MALS data was fitted to the Zimm and Berry model, fit order 1 for the molar mass and radius of gyration (R_g) analysis of different fractions in the GGM extract. The data from the first two and last two angles in the detector were not used due to noisy signals. When calculating molar mass, the values were compared with and without using detectors with band-pass filters. The input of the absorption and fluorescence effects induced by certain contaminants (e.g. lignin or lignin-derived phenolic residues) in the MALS derived molar mass data was controlled and corrected by a forward monitor done similarly by Zinovyev et al., 2018. Exponential fit with fit order up to 6 was used to obtain the fitted molar mass data. A higher fit order was necessary given the high size dispersity of samples.

The same buffer used during sample preparation, sodium citrate buffer at pH 4.5, was used as the eluent for AF4. The membrane used in AF4 was regenerated cellulose Ultracel with molecular weight cut off at 3 kDa from Merck KGaA (Darmstadt, Germany, which was obtained as square sheets (20 × 20 cm) and manually cut through the diagonal to fit in the channel.

2.3 Determination of *dn/dc*

The refractive index increment (*dn/dc*) of the samples was determined in batch mode using a dRI detector. Concentration series at 0.4, 0.6, 0.8, 1 and 1.2% w/v of sGGM and eGGM were prepared

and measurements were taken in triplicate. The obtained *dn/dc* values; 0.145 ± 0.001 and 0.148 ± 0.001 for sGGM and eGGM,, respectively were for MALS data processing.

2.4 AF4 conditions during method optimization

The separation of macromolecules during AF4 occurs on a thin channel, which contains porous ultrafiltration membrane. The channel consists of an impermeable upper plate and a permeable lower plate, separated by a spacer, which controls channel thickness. Sample analysis is performed in three steps: sample injection, sample relaxation/focusing and elution. During the injection and focusing steps, the sample is injected to accumulate very close to the membrane surface via a perpendicular flow. During the elution step, the sample analytes elute along the channel with a transverse channel flow in an increasing order of their diffusion coefficients (i.e., hydrodynamic sizes). The separation of analytes is obtained by applying a crossflow (V_c), which is perpendicular to the channel flow. V_c in a gradient (linear or exponential decay), a constant flow or a combination of thereof facilitate the separation in AF4.

In present study, sample injection flow and injection volume were 0.2 mL/min and 100 µl, respectively. The total focusing time included time for preparation of sample injection, sample injection, and sample focus. The channel thickness, sample injection and sample focus time during focusing step, V_c and flow gradients were optimized to achieve an efficient separation of GGM extracts (Table 1). Preparation of sample injection was kept constant for 1 min but sample injection and sample focus time was varied with a 5–10 min of total sample focusing time. The outflow/detector flow rate was kept constant at 1 mL/min.

2.5Small angle X-ray scattering (SAXS)

SAXS measurements were performed on 1% sGGM and eGGM solutions after mixing overnight in the same buffer as mentioned previously. In addition, to understand the structural features of GGM extracts subjected to various conditions, the solutions were heat treated to 70 ºC and measured after

cooling to RT. To understand the effect of mechanical shearing, both solutions were treated with high-shear mechanical mixing at 11000 rpm for 5 min using Ultraturrax (T-18 basic, IKA, Staufen, Germany) followed by three passes in a microfluidizer (Microfluidizer 110Y, Microfluidics, Westwood, MA, USA) at 800 bar. The shear-treated samples were shipped to the synchrotron facility where they were stored at RT. The sGGM solution was also measured after filtration using a 0.45 µm filter.

The SAXS experiments were conducted with at Diamond Light Source Synchrotron (Didcot, Oxfordshire, UK) with the standard solution SAXS set-up of beamLine B21 (bioSAXS robot), set to 20 ℃The distance between sample and detector (Pilatus 2M, Dectris, Baden-Daettwil, Switzerland) was 4.014 meters and the photon wavelength $\lambda = 0.100$ nm. The scattering vector q is defined as $q = \frac{4\pi \sin\theta}{\lambda}$, where θ is half of the scattering angle, and relates to distances in real space by $d = \frac{2\pi}{q}$. The obtained q-range was 0.032 to 3.8 nm^{-1} and the sample volume was 35 µl. Measurement times were 1 second per data frame, and 28 frames per sample. The calibration, normalization of data to an absolute scale, spherical averaging, merging and correction for background (buffer) scattering were done by in-house software and ScÅtter program version 3.1. The data were inspected for radiation damage before merging. For shear-treated samples, merging and correction for buffer scattering was done using MATLAB (MathWorks Inc, Natick, Massachusetts, U.S.A.).

2.6 Cryo-transmission electron microscopy

Cryo-transmission electron microscopy (Cryo-TEM) was performed on a 1% sGGM solution, prepared in the same way as described earlier. The solution was frozen after 1 hour of resting at 22 °C. The vitrified samples were prepared from 3 µl aliquots with a Leica EMGP vitrification device on freshly glow-discharged Quantifoil R1.2/1.3 grids. The samples were observed in a FEI Talos Arctica microscope operated at 200 kV. The images were recorded at a nominal magnification of 22,000x and 8500x with a FEI Falcon 3 camera operated in a linear mode.

3. Results and discussion

3.1 Method optimization in AF4

For the AF4 setup, we first tested the effect of channel thickness on the separation resolution. To further improve the data quality, sample focus duration was optimized. From our preliminary trials, these were the relevant key parameters. Using the optimized conditions, the molar mass, R_g and conformational properties for each separated fraction of GGM extracts were determined using MALS and dRI detectors.

The optimal fractionation of highly disperse GGM extracts required pre-optimization of crossflow rate, which are not presented in detail in this study. In the AF4-MALS analyses, the forward monitor in LS detectors helped to correct for light absorbance due to the presence of phenolic residues and/lignin that were heavily concentrated in some fractions of the GGM extracts. Band-pass filters in the MALS detectors were used to crosscheck for the overestimation of molar mass arising from fluorescence effects.

3.1.1 Effect of channel thickness

In AF4, a spacer determines the channel thickness, which affects the separation power. The spacer thickness can range from 50 to 500 µm; however, only a few dimensions are available commercially (e.g. Wyatt Technology Corporation provides only 250, 350 and 490 µm spacers). A thickness of 350 µm is most commonly used (Podzimek, 2011). Increased channel thickness has been reported to improve the separation of samples with a broad size distribution (Kim, Yang, & Moon, 2018). During preliminary trials, we observed a high size dispersity in both GGM extracts, especially in sGGM. Highly disperse nature of the extracts indicated that they most likely contained colloidal structures in addition to the dissolved polysaccharide chains. A broad distribution of molar mass due to the presence of oligosaccharides, polysaccharides and non-polysaccharide materials are a characteristic feature of crude polysaccharide extracts. To understand if increased channel thickness has an effect

on the separation resolution of highly heterogeneous samples like GGM extracts, we tested a 490 µm spacer inside the channel in addition to more commonly used 350 µm spacer.

For sGGM, using either the 350 and 490 µm spacer resulted in three fractions represented by three peaks in the dRI detector **(Fig. 1)**. Each fraction was associated with signals from UV and the MALS detector with varying intensities (a comparable figure is shown in **Fig. 2A**). With the 350 µm spacer, the molar mass of the small-sized fraction, i.e. the first peak in the fractogram was in the range of tens of 10^4 g/mol, in contrast in the order of 10,000 g/mol that was previously obtained from SEC (Valoppi et al., 2019). Using the 490 µm spacer, the molar mass of the smallest-sized fraction was reduced to the order of 10^4 g/mol and a distinct separation of the first and second fraction was observed. For these experiments with 490 µm spacer, V_c was increased to 3 mL/min from 2 mL/min. The latter was used with 350 µm spacer. During pre-optimization trials in 490 µm spacer, using V_c 2 mL/min and using the same method applied with 350 µm spacer, small-sized fraction was well separated, however, the separation of second and the third fraction separation was poor, and very large-sized analytes eluted only after the experimental run ended (data not shown). Separation resolution increases with increasing V_c and channel thickness. Hence, to maximize the separation power of these complex analytes, V_c 3mL/min was used in subsequent measurement with 490 µm spacer.

We speculated steric-hyperlayer elution and/ co-elution of large- and small-sized particles occurred with the 350 µm spacer, as the obtained molar mass of the first fraction seemed to originate from large-sized analytes in sGGM. With AF4, the normal mode of elution refers to the elution of analytes in an increasing order of their hydrodynamic radius. However, when analytes' size exceeds a certain diameter, due to predominant hydrodynamic lift forces on large-sized analytes, the normal mode of elution is reversed, referred to as a steric-hyperlayer mode of elution (Podzimek, 2011). Co-elution refers to the elution of mixtures of small- and large-sized analytes and has been previously observed in highly-branched amylopectin with $M_w > 10^7$ g/mol (Perez-Rea, Zielke, & Nilsson, 2017) and a

mixture of polymers with a broad molar mass distribution (Zielke et al., 2018). In disperse samples, the steric-hyperlayer mode can co-exist together with normal mode separation, and increase the dispersity of separated fractions (Podzimek, 2011). Co-elution, which is commonly observed in the steric transition region, was largely reduced in our study by increased channel thickness from the 490 µm spacer.

The effect of spacer thickness was also observed for eGGM, which consisted mainly of two fractions **(see Fig. 3B).** With the 350 µm spacer, separation of two fractions was achieved (data not shown); however, the molar mass of the first fraction could not be calculated precisely due to noisy light scattering (LS) signals (results not shown). With the 490 µm spacer, the LS data noises of the first fraction were reduced substantially due to better separation of different size classes (presented further). Hence, the 490 µm spacer was used in subsequent measurements of both sGGM and eGGM.

3.1.2 Effect of increased focus time

The molar mass of the first fraction of sGGM obtained with the 490 µm spacer was close to 10^4 g/mol. However, there were some noises in the signals and co-elution affected during the flow transition when V_c changed from a linear gradient to a steady V_c of 0.1 mL/min (between 20–30 min in **Fig. 1).** This was assumed to originate from the insufficient sample focusing in the thicker channel; thus, to further improve the elution, the effect of sample focusing duration was studied **(Fig. 2).** The focus time was increased from 5 min in a series by increasing the sample injection and focus duration (see **Table 1**).

With longer sample focusing, the noise in the LS signal reduced significantly (see the inset of Fig. 2A). Additionally, LS signal noises in the void region were also reduced. The molar mass of the small-sized fraction with 10 min total focusing step was now in the same range as in the previous study (Valoppi et al., 2019). Detailed characterization of each fraction is discussed in the section 3.2.1. In eGGM, with increased focus time, reduction in LS signal noises in the void region was

observed (data not shown). Sample focus time is directly proportional to the square of channel thickness and inversely proportional to the diffusion coefficient of analyte. This means in thicker channels large particles need a longer focus time compared to the small particles (Podzimek, 2011).

An efficient fractionation of GGM extracts was achieved using the 490 µm spacer, with channel thickness and focus time playing significant role. However, this came with a loss in sample recovery. The total mass recovery with 490 µm spacer thickness and 3 mL/min crossflow rate was approximately 45–50 % (sGGM) and 43 % (eGGM) and versus 60 % (sGGM) and 68 % (eGGM) with 350 µm spacer and 2 mL/min crossflow rate for sGGM. However, with the current setup, an efficient separation of distinctly different sized analytes was observed, which the focus of this current study was. To improve recovery, using even lower cut-off membrane than currently used 3 kDa and a different membrane material for e.g. polyethersulfone are worth investigating. Additionally, the recovery calculation will also be affected from the *dn/dc* value, if different size-fractions have heterogeneity in chemical composition.

3.1.3 Challenges in AF4 characterization of crude extracts of polysaccharides

AF4 is the most instrumentally developed field-flow fractionation method to characterize a wide range of natural and synthetic polymers, colloidal particles, and various biological and environmental samples (Podzimek, 2011). It is possibly the most suitable method for the characterization of complex mixtures of samples with a broad size distribution and ultra-high molar mass polymers and particles (Podzimek, 2011). In our context, AF4 coupled with UV, MALS and dRI detectors gave comprehensive information of both GGM extracts on the presence of multiple-sized fractions, their molar mass, conformational properties, and fraction composition (UV-absorbing compounds), which was impossible to obtain with conventional SEC. Hence, this method can be successfully employed for the characterization of crude polymer extracts. In order to facilitate the use of AF4 to fractionate

highly disperse samples, like GGM extracts, we would like to highlight some issues that we encountered during method optimization.

1) The fractionation of highly disperse samples with a very broad size distribution is often challenging in a single run, which is otherwise a favorable approach. For efficient fractionation, pre-trials using a combination of linear/exponential gradients and a steady crossflow need to be performed.

2) In samples with a broad molar mass distribution, a high sample injection load is required to characterize the small-sized fractions; however, injection of a higher load may lead to problems of channel overloading and sample aggregation, which needs to be considered.

3) For any given channel thickness, the separation resolution increases with increasing V_c and channel flow rate. However, a high V_c prolongs the experimental run time and increases channel pressure resulting in leakage problems particularly in thin channels. Thicker channels offer several advantages for characterizing crude polymer extracts. Shear rates are low, which is particularly advantageous for studying loose polysaccharides aggregates. Analytes are diluted, preventing the risk of aggregation, when a higher sample volume is required during injection as mentioned earlier. In addition, the possibility of sample-membrane interaction is lower in thick channels than in thin channel, which would have a positive effect in recovery (Wahlund, 2013). The steric inversion diameter can be increased with increased channel thickness. The increase in steric inversion diameter reduces the co-elution and steric-elution phenomenon in size disperse samples such as crude polysaccharide extracts.

3.2 Macromolecular properties of GGM extracts

3.2.1 Molar mass analysis

Both types of GGM extracts were previously characterized as low-molar mass polysaccharides with molar mass around 8,000 in DMSO and 12,000 g/mol in aqueous solvent— both analyzed by SEC. According to our visual observations of the opaque sGGM solution and translucent eGGM solution, and our recent study on the aggregation behavior of eGGM (Bhattarai et al., 2020) it was hypothesized that larger structures existed in the GGM solutions. Hence, advanced fractionation method such as AF4 was required to understand the complete and complex macromolecular profile of GGM extracts. The optimized AF4 method in previous section was used to fractionate and characterize the macromolecular features of sGGM and eGGM, which are discussed here.

The dRI, UV and LS signal peaks indicated that sGGM was more disperse with three distinct fractions compared to only two fractions in eGGM—each represented by a peak **(Fig. 3A and B)**.

In both types of GGM extracts, the most abundant fraction had molar mass between 1-1.3×10^4 g/mol **(Fig. 3C and D; Table 2)**, similar to those reported in previous studies. The R_g of this fraction could not be calculated precisely as low-molar mass analytes do not show angular dependency of scattered light (Podzimek, 2011). This fraction did not show significant concentration dependency, suggesting that they were not aggregated polysaccharides. The slightly higher molar mass obtained in 0.5% sGGM was most likely due to low LS signals because of low concentration. The second fraction in both types of GGM extracts had a molar mass in the range of 10^6–10^7 g/mol. Concentration dependency was observed between 0.5% and 1% eGGM; however, this again was most likely due to low LS signals in 0.5% eGGM. The third fraction in sGGM (not present in eGGM) was in the range of 10^{10}g/mol at both concentrations.

The dRI, UV and LS detectors coupled to AF4 provided information on the amount, presence of UV-absorbing compounds, and the size/molar mass of each separated fraction, respectively **(Fig. 3A and B)**. In both GGM extracts, a UV signal at varying intensities was associated with each peak/size-class. In sGGM, the ratio of dRI, UV and LS peak areas between the first, second and the third fraction

was 9.7:1.7:1 (dRI), 1:2.7:2.4 (UV) and 0.03:2.8:97.2 (LS), respectively. The distribution of UV-absorbing compounds between the three fractions in sGGM was interesting. The second and third fraction contained a high amount of UV-absorbing compounds, but the first fraction had only a low amount. In eGGM, the ratio of RI, UV and LS peak areas between the first and the second fraction was 6.5:1 (dRI), 1:1.1 (UV), and 1:99 (LS), respectively. This indicates that equal amounts of UV-absorbing compounds were present in both size-classes, despite low molar mass polysaccharides were being the most abundant. Co-extracted lignin-derived phenolic residues and extractives are most likely the source of these UV signals (Mikkonen et al., 2019) and the high UV signal intensity in sGGM compared to eGGM in Fig. 3 was also in agreement with the total phenolic content result. Our recent study showed that these phenolic residues could be in polymerized form as lignin (Lahtinen et al., 2019; Valoppi et al., 2019).

From the molar mass analysis, it was concluded that in addition to low-molar mass polysaccharides (likely individually dissolved molecules), both GGM extracts contained fractions of a higher structural order, especially in sGGM. The molar mass of the second most abundant fraction of sGGM, which was in the range of 10^7 g/mol, has been previously reported in pure polysaccharide such as dextrans (Maina et al., 2014) and aggregates from beta-glucan (Zielke, 2017). However, in contrast with pure polysaccharides GGM-rich wood extracts contain other components, e.g., lignin, which could give rise to colloidal particles and thus complicate direct comparisons. The extremely high molar mass of the third fraction, which was the least abundant of the three fractions, suggested the presence of particles, instead of dissolved polysaccharides. In such cases, molar mass becomes an irrelevant parameter. The fraction in eGGM with the obtained molar mass in the range of 10^6-10^7 g/mol can be assigned to previously observed aggregates of eGGM (Bhattarai et al., 2020). Kishani, Vilaplana, Xu, Xu, and Wågberg (2018) have also reported that GGM obtained from TMP process forms aggregates in solution. Hence, we expect that the second fraction observed for eGGM in our current study likely originate from the association of the polysaccharides. To understand the

conformational properties of the second and third fraction of sGGM, we studied these fractions separately as discussed in the next section.

3.2.2 Conformational properties

To understand the conformational properties of the second and third fraction of sGGM, R_g was plotted as a function of molar mass **(Fig. 4).** The results were complemented with SAXS and Cryo-TEM. The second fraction of eGGM had much lower intensity of LS signal compared to sGGM; hence, such plot was not obtained.

The R_g of the second sGGM fraction was < 50 nm, and the major part of this fraction was estimated to have R_g< 10 nm. This indicates the presence of highly compact structures, considering the molar mass of this fraction was in the range of 10^7 g/mol. The conformation plot of this fraction where R_g was > 10 nm gave a slope of 0.77, which is a typical feature of random coils. From the third sGGM fraction, a slope of 0.27 was obtained, which is close to what is known for spheres (0.33) (Podzimek, 2011).

Cryo-TEM was performed as a visualization tool at high-resolution in sub-micron range (**Fig. 5**) to confirm the conformational information obtained from AF4-MALS. The sGGM solution under the TEM showed two different features: a network of loose aggregates, where dense-objects appeared to be embedded, forming a core-shell-like network (**Fig.5A and B**) and noticeable sub-micron sized spherical particles **(Fig. 5C and D)**. Similar structure was observed previously in eGGM (Bhattarai et al., 2020).

SAXS was performed on both sGGM and eGGM solutions **(Fig. 6)** to obtain any further structural information to validate the conformational information obtained from AF4-MALS **(Fig. 4)** and Cryo-TEM (**Fig. 5**). In sGGM solution a characteristics feature in the region of $q \approx 0.1$ nm^{-1} corresponding to real space distance ~ 60 nm was observed **(shoulder in Fig. 6A)**, which indicated structural features in the respective length scale. The shoulder was persistent after the high-intensity mechanical

shearing of the sGGM solution and even after filtration of the solution through a 0.45 μm filter. Heat treatment reduced this shoulder to some extent. Thus, we expect that the shoulder represents sGGM aggregates or particles or their combination, corresponding with the second fraction obtained from AF4 and possibly observed under TEM **(Fig. 5A and B)**. This fraction may be partially broken or dissolved during treatment such as high-intensity shearing, and re-assembled when resting. Conversely, such features were not pronounced in eGGM. The normalized scattering intensity of sGGM solution was significantly higher at high *q*-range **(Fig. 6)**, indicating more scattering structures in the corresponding length-scale.

The present results indicated that besides low-molar mass polysaccharide fraction, sGGM consisted of compact structures in different size-scales. The core-shell-like features observed in sGGM under TEM is analogous to hybrid micro-gels (Karg & Hellweg, 2009). Our recent study employed a batch centrifugation approach to fractionate different size-classes in sGGM. The size characteristics of the third fraction from the present study matched with those of the pellet obtained previously after centrifugation, which was identified as primarily composed of lignin (Valoppi et al., 2019) with a molar mass around 3000 g/mol in DMSO. This explains the particle-like conformation of the third fraction, as lignin has poor solubility in aqueous solvents. The observed particle morphology in **Fig. 5C and D** differed from pure lignin nanoparticles, as the latter have defined edges (Bai et al., 2019; Lievonen et al., 2016). The pellet also consisted of about 25% of the total polysaccharides of sGGM (Valoppi et al., 2019); hence, we suggest that the outer shell of the present particles observed under TEM could be composed of GGM polysaccharides, and the inner core from lignin, due to the differences in the hydrophilicity of polysaccharides and lignins. Analogous to hybrid micro-gel structures, lignin could crosslink with polysaccharides and form such a core-shell like structure. This could also support the presence of lignin carbohydrate complexes, which has been recently identified in sGGM (Lahtinen et al., 2019).

We have previously observed that the lignin-rich fraction with particle size between 20–600nm (peak maxima at 120 nm) can contribute to the emulsion stabilization capacity of sGGM (Valoppi et al., 2019). From the present study, it can be concluded that the second and third fractions that were presumed to be effective in emulsions, were indeed colloidal particles. This type of emulsion stabilization is referred to as Pickering-type emulsion stabilization (Pickering, 1907). Use of Pickering emulsions stabilized by insoluble biopolymers such as cellulose, lignin, starch, and chitin, for food, pharmaceuticals and other technical applications have gained popularity in the last decade (Bai et al., 2019; Dickinson, 2017). The loose network-like structure observed under TEM indicates that not all of the observed particles existed as individually, but rather embedded in an aggregated network of GGM.

Both types of GGM extracts showed interesting conformational properties. The presence of colloidal entities like aggregates and particles may exhibit functionality as particle fillers, creating stable dispersed multiphasic systems. Our results lead to important new research questions, such as the effect of pH, ionic strength, and organic solvents on the macromolecular and conformational properties of GGM extracts.

4 Conclusion

Recovery and valorization of hemicelluloses for future applications requires knowledge of their solution properties in aqueous state, which mandates their efficient fractionation and characterization. The present study optimized the AF4 method for the separation of different size-classes and the subsequent characterization of GGM-rich wood extracts obtained from an aqueous based extraction method—PHWE.

Both types of GGM-rich extracts (sGGM and eGGM) were primarily heterogeneous mixtures of polysaccharide–particle or polysaccharide–aggregate systems together with individually dissolved polysaccharides. The crude sGGM extract consisted of a low-molar mass polysaccharide fraction and

compact polysaccharide–lignin nanoparticles in the nano- and sub-micron scale. These colloidal particles were absent in the ethanol-precipitated GGM—very likely due to removal of major portion of phenolics compounds; however, colloidal assemblies existed. For the first time, the present study provided a comprehensive overview of the complex macromolecular features of GGM-rich extracts and a comparison between the colloidal properties of GGM with two different grades of purity. The optimized AF4 method in the present study will facilitate the characterization of highly disperse crude polysaccharide extracts without pre-fractionation, which is often challenging. Comprehensive characterization of carbohydrate extracts facilitates their application as novel biomass-based materials, especially as multi-mechanistic stabilizers obtained from soluble and less soluble molecules. The obtained results will also facilitate biorefineries to conduct need-based carbohydrate extraction.

Funding Sources

The doctoral programme of Food Chain and Health at the University of Helsinki and EU-COST Action FP1306 are acknowledged for funding MB and her scientific visit to the University of Natural Resources and Life Sciences, Austria, respectively. Väisälä Fund is acknowledged for funding the travel Inkeri Kontro to Diamond Light Source Synchrotron in UK.

Conflict of interest

There are no conflicts of interest to declare.

Acknowledgement

We thank Dr. Petri Kilpeläinen at the Natural Resource Institute Finland for providing GGM extracts. Dr. Stefan Böhmdorfer and Dr. Ivan Sumersky at the University of Natural Resources and Life

Sciences, Austria, are acknowledged for technical assistance during AF4 measurements. Benita Löflund, and Pasi Laurinmäki, University of Helsinki, are acknowledged for technical assistance in performing Cryo-TEM imaging, which was carried out with the support of Biocenter Finland and the Instruct-FI CryoEM core facility, University of Helsinki. Dr. Fabio Valoppi is acknowledged for assistance during sample preparation for synchrotron experiments at Diamond Light Source Synchrotron Facility. Julia Varis is acknowledged for her help to draw the graphical abstract.

CRediT authorship contribution statement

Mamata Bhattarai: Conceptualization, Methodology, Investigation, Formal analysis, Visualization, Writing-original manuscript draft

Irina Sulaeva: Methodology, Formal analysis, Validation, Writing-Review and Editing

Leena Pitkänen: Conceptualization, Formal analysis, Validation, Writing-Review and Editing

Inkeri Kontro: Investigation, Formal analysis, Writing-Review and Editing

Maija Tenkanen: Conceptualization, Methodology, Writing-Review and Editing

Antje Potthast: Methodology, Supervision, Writing-Review and Editing

Kirsi S. Mikkonen: Conceptualization, Supervision, Writing-Review and Editing

REFERENCES

Al-Rudainy, B., Galbe, M., Arcos Hernandez, M., Jannasch, P., & Wallberg, O. J. P. (2019). Impact of lignin content on the properties of hemicellulose hydrogels. *Polymers,* 11(1), 35.

Alakalhunmaa, S., Parikka, K., Penttilä, P. A., Cuberes, M. T., Willför, S., Salmén, L., & Mikkonen, K. S. (2016). Softwood-based sponge gels. *Cellulose,* 23(5), 3221-3238.

Bai, L., Greca, L. G., Xiang, W., Lehtonen, J., Huan, S., Nugroho, R. W. N., . . . Rojas, O. J. (2019). Adsorption and Assembly of Cellulosic and Lignin Colloids at Oil/Water Interfaces. *Langmuir,* 35(3), 571-588.

Bhattarai, M., Pitkanen, L., Kitunen, V., Korpinen, R., Ilvesniemi, H., Kilpelainen, P. O., . . . Mikkonen, K. S. (2019). Functionality of spruce galactoglucomannans in oil-in-water emulsions. *Food Hydrocolloids,* 86, 154-161.

Bhattarai, M., Valoppi, F., Hirvonen, S. P., Hietala, S., Kilpelainen, P. O., Aseyev, V., & Mikkonen, K. S. (2020). Time-dependent self-association of spruce galactoglucomannans depends on pH and mechanical shearing. *Food Hydrocolloids,* 102, 105607.

Chadni, M., Grimi, N., Bals, O., Ziegler-Devin, I., & Brosse, N. (2019). Steam explosion process for the selective extraction of hemicelluloses polymers from spruce sawdust. *Industrial Crops and Products,* 141, 111757.

Chadni, M., Grimi, N., Ziegler-Devin, I., Brosse, N., & Bals, O. (2019). High voltage electric discharges treatment for high molecular weight hemicelluloses extraction from spruce. *Carbohydrate Polymers,* 222, 115019.

Dickinson, E. (2017). Biopolymer-based particles as stabilizing agents for emulsions and foams. *Food Hydrocolloids,* 68, 219-231.

Ebringerová, A., Hromádková, Z., & Heinze, T. (2005). *Hemicellulose*. In T. Heinze (Ed.), *Polysaccharides I: Advances in Polymer Science* (pp. 1-67). Berlin: Springer

Employment, M. o. E. A. a. Wood based Bioeconomy Solving Global challanges.(2017). **www.bioeconomy.fi/publication-wood-based-bioeconomy-solving-global-challenges/,** Accessed 14th August.2017.

Guo, M. Q., Hu, X., Wang, C., & Ai, L. (2017). *Polysaccharides: Structure and Solubility*. In *Solubility of Polysaccharides*. London, United Kingdom: IntechOpen Limited

Harding, S. E. (2005). *Analysis of Polysaccharides by Ultracentrifugation. Size, Conformationand Interactions in Solution*. In T. Heinze (Ed.), *Polysaccharides I: Structure, Characterization and Use* (pp. 211-254). Berlin, Heidelberg: Springer Berlin Heidelberg

Jedvert, K., Saltberg, A., Lindström, M. E., & Theliander, H. (2012). Mild steam explosion and chemical pre-treatment of Norway spruce. *BioResources,* 7(2), 2051-2074.

Karg, M., & Hellweg, T. (2009). New "smart" poly(NIPAM) microgels and nanoparticle microgel hybrids: Properties and advances in characterisation. *Current Opinion in Colloid & Interface Science,* 14(6), 438-450.

Kilpeläinen, P. O., Hautala, S. S., Byman, O. O., Tanner, L. J., Korpinen, R. I., Lillandt, M. K. J., . . . Ilvesniemi, H. S. (2014). Pressurized hot water flow-through extraction system scale up from the laboratory to the pilot scale. *Green Chemistry,* 16(6), 3186-3194.

Kim, Y. B., Yang, J. S., & Moon, M. H. (2018). Investigation of steric transition with field programming in frit inlet asymmetrical flow field-flow fractionation. *Journal of Chromatography A,* 1576, 131-136.

Lahtinen, M. H., Valoppi, F., Juntti, V., Heikkinen, S., Kilpeläinen, P. O., Maina, N. H., ... (2019). Lignin-Rich PHWE Hemicellulose Extracts Responsible for Extended Emulsion Stabilization. *Frontiers in Chemistry,* 7, 871.

Lehtonen, M., Merinen, M., Kilpeläinen, P. O., Xu, C., Willför, S., & Mikkonen, K. S. (2018). Phenolic residues in spruce galactoglucomannans improve stabilization of oil-in-water emulsions. *Journal of Colloid and Interface Science,* 512, 536-547.

Lehtonen, M., Teräslahti, S., Xu, C., Yadav, M. P., Lampi, A.-M., & Mikkonen, K. S. (2016). Spruce galactoglucomannans inhibit lipid oxidation in rapeseed oil-in-water emulsions. *Food Hydrocolloids,* 58, 255-266.

Lievonen, M., Valle-Delgado, J. J., Mattinen, M.-L., Hult, E.-L., Lintinen, K., Kostiainen, M. A., . . . Österberg, M. (2016). A simple process for lignin nanoparticle preparation. *Green Chemistry,* 18(5), 1416-1422.

Lindblad, M. S., Dahlman, O., Sjöberg, J., & Albertsson, A.-C. (2009). *Modified galactoglucomannans from forestry waste-water for films and hydrogels*. In *Polysaccharide Materials: Performance by Design*: ACS Publications

Maina, N. H., Pitkänen, L., Heikkinen, S., Tuomainen, P., Virkki, L., & Tenkanen, M. (2014). Challenges in analysis of high-molar mass dextrans: Comparison of HPSEC, AsFlFFF and DOSY NMR spectroscopy. *Carbohydrate Polymers,* 99, 199-207.

Mikkonen, K. S., Heikkilä, M. I., Willför, S. M., & Tenkanen, M. (2012). Films from glyoxal-crosslinked spruce galactoglucomannans plasticized with sorbitol. *International Journal of Polymer Science,* 2012, 8.

Mikkonen, K. S., Kirjoranta, S., Xu, C., Hemming, J., Pranovich, A., Bhattarai, M., . . . Willför, S. (2019). Environmentally-compatible alkyd paints stabilized by wood hemicelluloses. *Industrial Crops and Products,* 133, 212-220.

Mikkonen, K. S., Merger, D., Kilpeläinen, P., Murtomäki, L., Schmidt, U. S., & Wilhelm, M. (2016). Determination of physical emulsion stabilization mechanisms of wood hemicelluloses via rheological and interfacial characterization. *Soft Matter,* 12(42), 8690-8700.

Mikkonen, K. S., Xu, C., Berton-Carabin, C., & Schroën, K. (2016). Spruce galactoglucomannans in rapeseed oil-in-water emulsions: Efficient stabilization performance and structural partitioning. *Food Hydrocolloids,* 52, 615-624.

Perez-Rea, D., Zielke, C., & Nilsson, L. (2017). Co-elution effects can influence molar mass determination of large macromolecules with asymmetric flow field-flow fractionation coupled to multiangle light scattering. *Journal of Chromatography A,* 1506, 138-141.

Pickering, S. U. (1907). CXCVI.—Emulsions. *Journal of the Chemical Society, Transactions,* 91(0), 2001-2021.

Pitkänen, L., Tenkanen, M., & Tuomainen, P. (2011). Behavior of polysaccharide assemblies in field-flow fractionation and size-exclusion chromatography. *Analytical and Bioanalytical Chemistry,* 399(4), 1467-1472.

Podzimek, S. (2011). *Asymmetric Flow Field Flow Fractionation*. In *Light Scattering, Size Exclusion Chromatography and Asymmetric Flow Field Flow Fractionation* (pp. 259-305)

Runyon, J. R., Ulmius, M., & Nilsson, L. (2014). A perspective on the characterization of colloids and macromolecules using asymmetrical flow field-flow fractionation. *Colloids and Surfaces A: Physicochemical and Engineering Aspects,* 442, 25-33.

Schoultz, S. V. (2015). Method for extracting biomass. In U. S. P. a. T. Office (Ed.), *Google Patents*. US: CH-Bioforce Oy.

Sjöström, E. (1993). *Wood chemistry: fundamentals and applications*: Gulf professional publishing.

Söderqvist Lindblad, M., Ranucci, E., & Albertsson, A. C. (2001). Biodegradable polymers from renewable sources. New hemicellulose-based hydrogels. *Macromolecular Rapid Communications,* 22(12), 962-967.

Sundberg, A., Sundberg, K., Lillandt, C., & Holmhom, B. (1996). Determination of hemicelluloses and pectins in wood and pulp fibres by acid methanolysis and gas chromatography. *Nordic Pulp & Paper Research Journal,* 11(4), 216.

Valoppi, F., Lahtinen, M., Bhattarai, M., Kirjoranta, S. J., Juntti, V. K., Peltonen, L., . . . Mikkonen, K. S. (2019). Centrifugal fractionation of softwood extracts improves biorefinery workflow and yields functional emulsifiers. *Green Chemistry,* 21, 4691-4705.

Wahlund, K.-G. (2013). Flow field-flow fractionation: Critical overview. *Journal of Chromatography A,* 1287, 97-112.

Westbye, P., Köhnke, T., Glasser, W., & Gatenholm, P. (2007). The influence of lignin on the self-assembly behavior of xylan rich fractions from birch *(Betula pendula)*. *Cellulose,* 14, 603-613.

Willför, S., Rehn, P., Sundberg, A., Sundberg, K., & Holmbom, B. (2003). Recovery of water-soluble acetylgalactoglucomannans from mechanical pulp of spruce. *Tappi Journal,* 2(11), 27-32.

Xu, C., Willfor, S., Sundberg, K., Pettersson, C., & Holmbom, B. (2007). Physico-chemical characterization of spruce galactoglucomannan solutions: stability, surface activity and rheology. *Cellulose Chemistry Technology,* 41(1), 51.

Zielke, C. (2017). On the Aggregation of Cereal β-Glucan and its Association with other Biomolecules: A Study using Asymmetric Flow Field-Flow Fractionation (AF4). *Department of Food Technology* (Vol. Doctor of Philosophy, p. 195). Lund: Lund University.

Zielke, C., Fuentes, C., Piculell, L., & Nilsson, L. (2018). Co-elution phenomena in polymer mixtures studied by asymmetric flow field-flow fractionation. *Journal of Chromatography A,* 1532, 251-256.

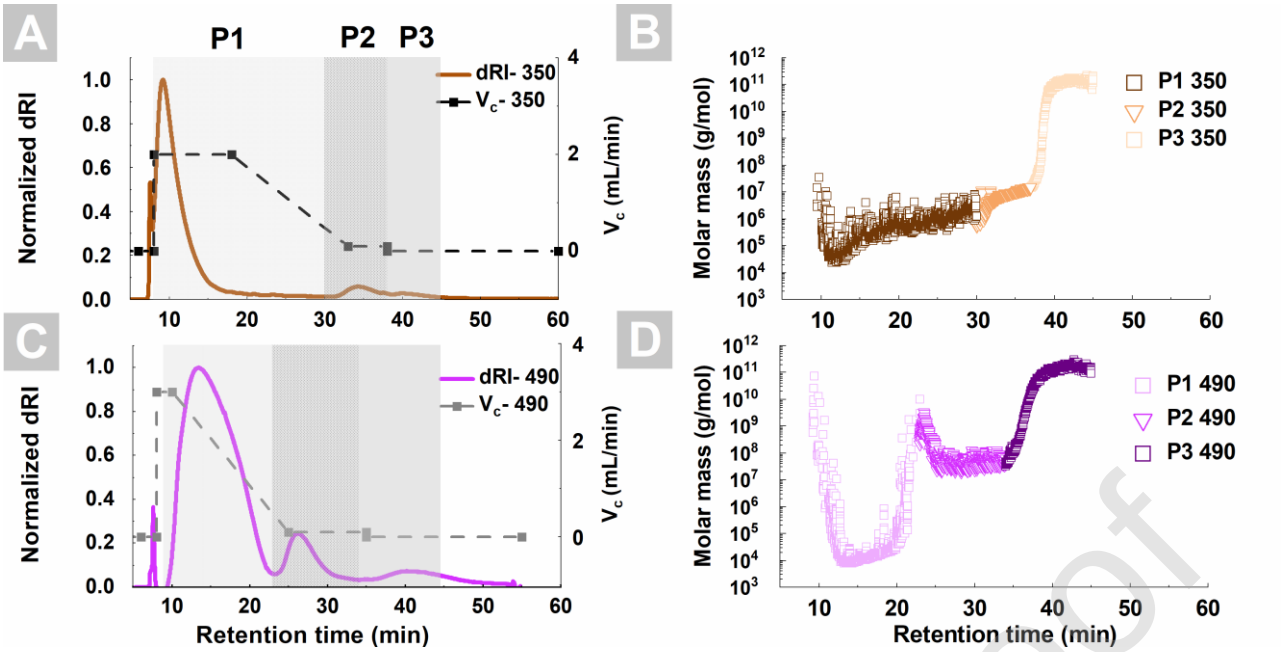

Fig. 1. (A, C) Normalized dRI signal intensity versus retention time of 1% sGGM separated with a 350 and 490 µm spacer presented together with the applied crossflow rate (V_c) during separation. **(B, D)** Corresponding molar mass obtained from the three peaks (P1, P2 and P3) obtained in panels A and C. Zimm model was used for P1 and Berry model was used for P2 and P3. Panels A and C and panels B and D share the same x-axis.

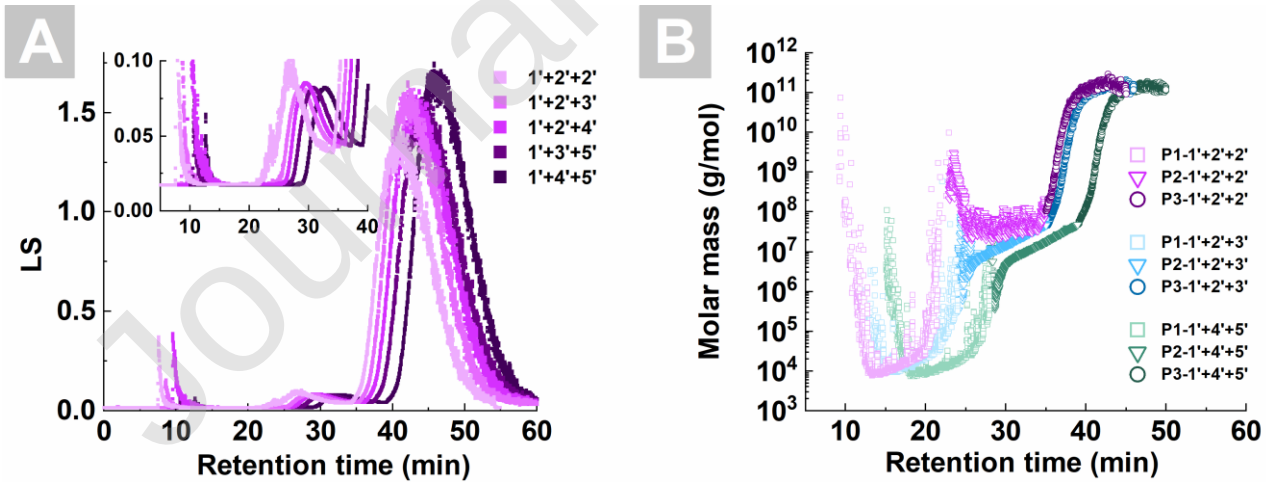

Fig. 2. (A) Absolute LS signal (V) intensity of 1% sGGM separated on a 490 µm spacer focused for different times. The inset in panel A shows the magnified LS signals in the corresponding retention

time. In the legend, 1'+2'+2' indicate 1 min of preparation for sample injection, 2 min of sample injection and 2 min of sample focus, for example. **(B)** Corresponding molar mass of the three peaks (P1, P2 and P3) from different sample focus times. Zimm model was used for P1 and Berry model was used for P2 and P3.

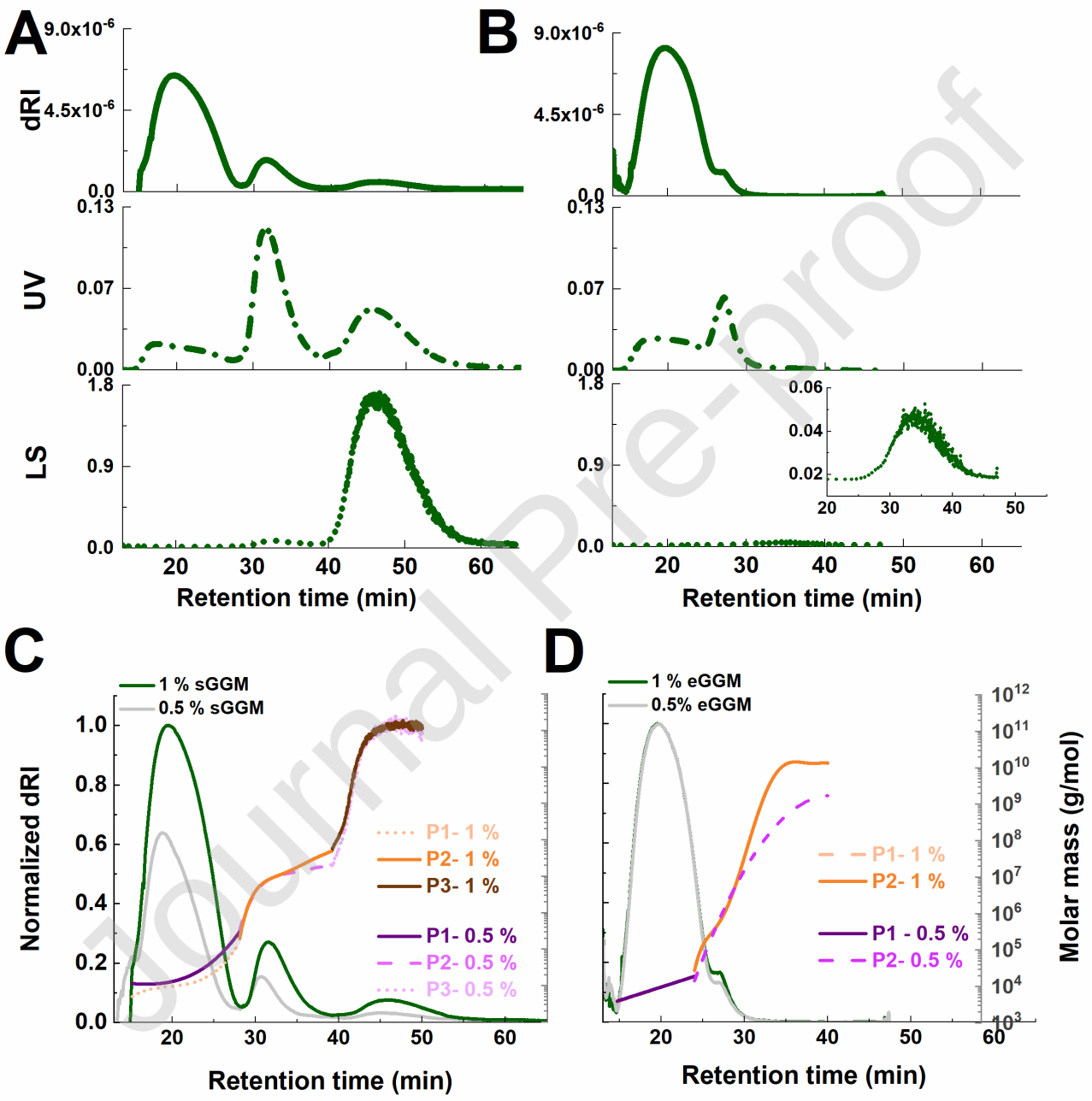

Fig. 3. dRI (RIU), UV (V) and LS (V) signals in absolute units versus retention time of 1% (A) sGGM and (B) eGGM dissolved overnight in 25 mM citrate buffer at pH 4.5. The inset in panel B

shows the magnified LS signal of 1% eGGM for the corresponding retention time. Normalized dRI signal intensity versus retention time of 0.5 and 1% (C) sGGM and (D) eGGM with fitted molar mass (g/mol) for each eluted peak. Zimm model was used for P1 and Berry model was used for P2 and P3 (when applicable). Spacer- 490 μm, total focusing time- 10 min. In panels C and D, each chromatogram was normalized against its highest magnitude. The right and left axes of panel C and D share the same axis.

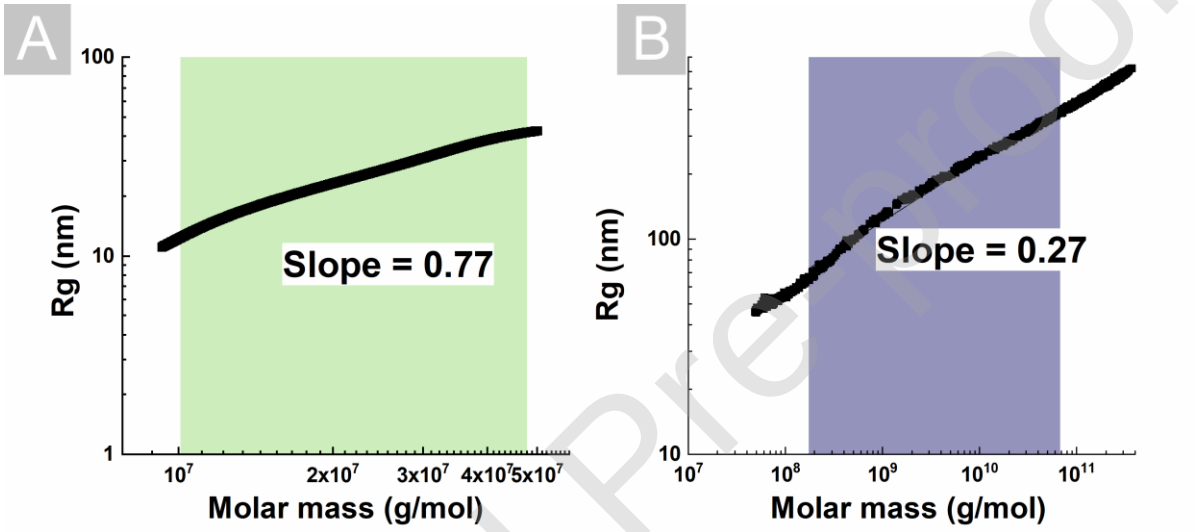

Fig. 4. Log-log plot of radius of gyration (R_g) versus molar mass of the (A) 2nd and (B) 3rd peak of 1% sGGM. Refer to Fig. 3 A and C for the peaks. The slopes obtained from the shaded area are labeled in the figure.

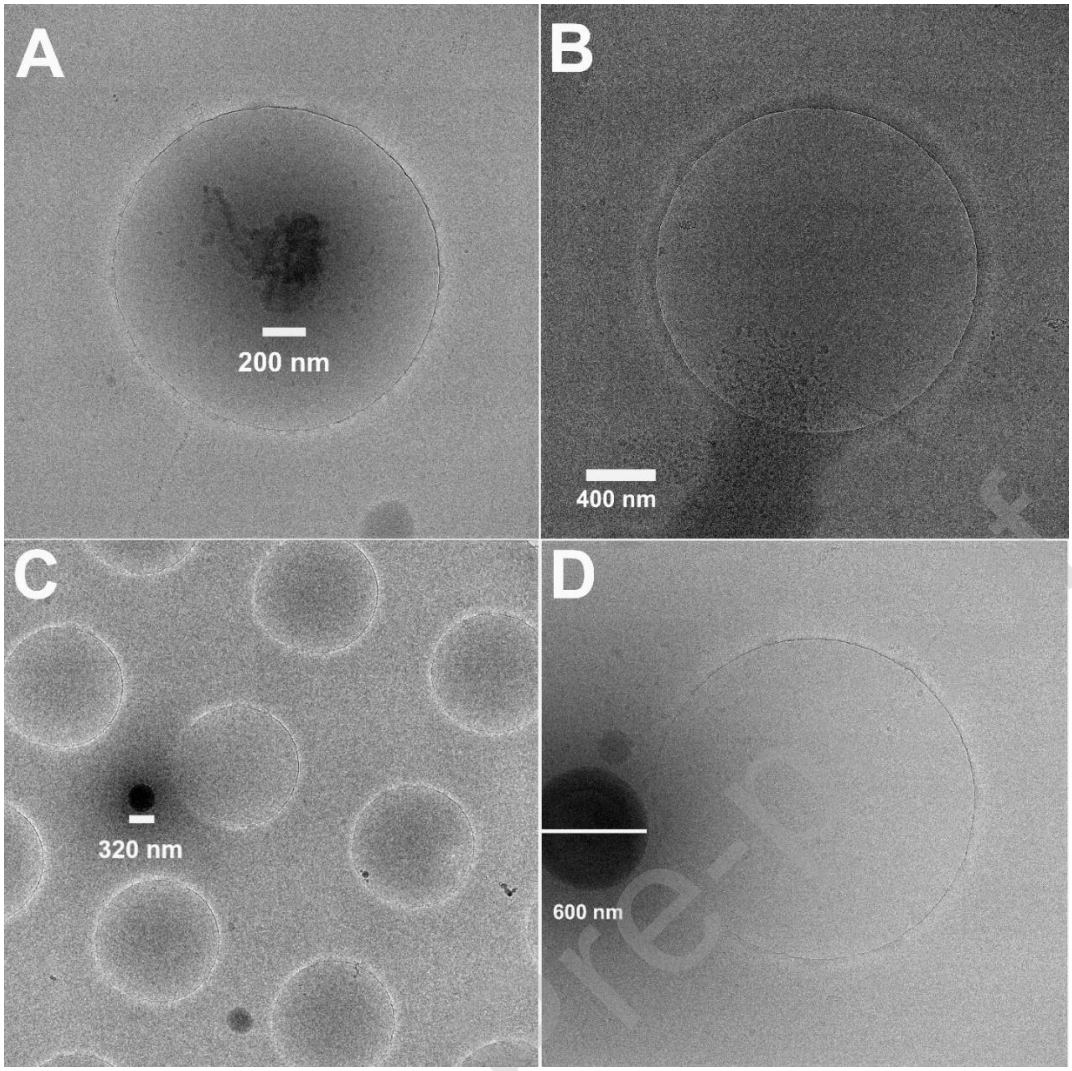

Fig. 5. (A, B, C, D) Cryo-TEM images of the 1% sGGM dissolved in 25 mM sodium citrate buffer overnight at pH 4.5.Note: the light-colored round circles in the images originate from the sample holder. Image B was processed for better contrast to visualize the aggregates. In image C, only the dark particle with a scale bar beneath is from the sample.

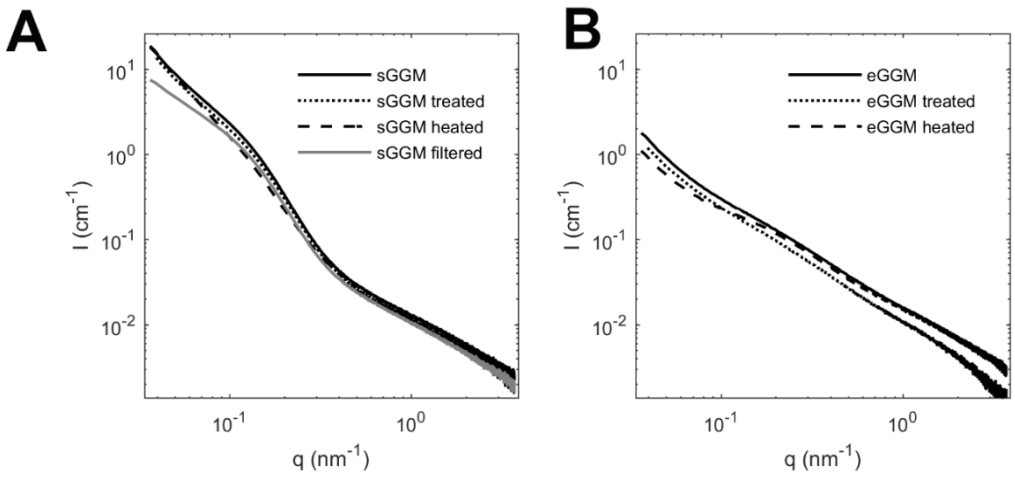

Fig. 6. SAXS intensity plotted as a function of scattering vector of 1% (A) sGGM solution without any treatment (sGGM), homogenized (sGGM-treated), heated to 70 ºC (sGGM-heated) and filtered through 0.45 µm (sGGM-filtered) (B) eGGM solution without shear treatment (eGGM), shear-treated (eGGM-treated), and heated to 70 °C (eGGM-heated).

Table 1. Summary of membrane, spacer thickness (µm) and total focusing time (min) studied during optimization of AF4 of GGM extracts. Total focusing time included time for preparation for sample injection, sample injection and sample focus, in series. The crossflow rate (V_c) in mL/min during the elution steps (I-IV) and duration (min) of each step is presented. Note: Step II operates under linear gradient of V_c.

Sample	**Spacer thickness**	**Total focusing time**	**Step I**	**Step II**	**Step III**	**Step IV**
			V_c **(Duration)**	V_c **(Duration)**	V_c **(Duration)**	V_c **(Duration)**
sGGM	350	5 (1'+2'+2')	2–2 (10)	2–0.1 (15)	0.1–0.1 (5)	0–0 (10)
sGGM	490	5 (1'+2'+2') 6 (1'+2'+3') 7 (1'+2'+4') 9 (1'+3'+5') 10 (1'+4'+5')	3–3 (2)	3–0.1 (15)	0.1–0.1 (10)	0–0 (20)
eGGM	490	10 (1'+4'+5')	n/a (n/a)	3–0 (15)	0–0 (20)	n/a (n/a)

n/a – Not applicable

Note: (1'+2'+2') means 1 min of preparation for sample injection, 2 min of sample injection and 2 min of sample focus, for example.

Table 2 Weight-average molar mass (M_w), number-average molar mass (M_n) in g/mol, polydispersity index (PDI), z-average radius of gyration (R_g) in nm of different fractions of 0.5 and 1% sGGM and eGGM. The molar mass was calculated by integrating the eluted peaks in **Fig. 3A and B**. Fit order and R^2 to obtain molar mass (M_w and M_n) and R_g presented for each fraction.

Sample	**1st fraction (Fit order, R^2)**			**2nd fraction (Fit order, R^2)**				**3rd fraction (Fit order, R^2)**			
	M_w	**M_n**	**PDI**	**M_w**	**M_n**	**PDI**	**R_g**	**M_w**	**M_n**	**PDI**	**R_g**
0.5 % sGGM	2.1×10^4	1.5×10^4	1.44	8.0×10^6	3.8×10^6	2.1	nd	8.7×10^{10}	3.6×10^8	242.5	494.6
	Exp 3, 0.64			Exp 4, 0.99				(n/a)			(n/a)
1 % sGGM	1.3×10^4	1.1×10^4	1.27	1.1×10^7	5.7×10^6	2.0	15.7	9.8×10^{10}	1.3×10^9	75.8	440.8
	Exp 3, 0.86			Exp 6, 0.99			Exp 2, 0.94	(n/a)			(n/a)
0.5 % eGGM	1.0×10^4	8.9×10^3	1.15	2.5×10^6	5.2×10^4	48.27	n/a	n/a			
	Exp 1, 0.94			Exp 2, 0.97							
1 % eGGM	1.0×10^4	8.8×10^3	1.16	9.4×10^7	1.2×10^5	786.89	n/a	n/a			
	Exp 1, 0.82			Exp 6, 0.98							

n/a= Not applicable. nd= not determined due to noisy signal

Note: R_g of 1st fraction could not be determined. The 3rd fraction and a part of 2nd fraction of sGGM most likely originate from particles and/ aggregates, hence the molar mass values presented do not represent individual polysaccharide molecules.